Experimental and Computational Study of the Kinetics of OH + Pyridine and Its Methyl- and Ethyl-Substituted Derivatives

Laurence Y. Yeung and Matthew J. Elrod*

Department of Chemistry, Oberlin College, Oberlin, Ohio 44074

Received: November 5, 2002; In Final Form: April 1, 2003

The overall rate constants for the reaction of OH with pyridine, its three monosubstituted methyl derivative isomers (the picolines), its six disubstituted methyl derivative isomers (the lutidines), and its three monosubstituted ethyl derivative isomers have been measured using the turbulent flow technique with high-pressure chemical ionization mass spectrometry at 100 Torr pressure and 298 K. A structure−reactivity relationship model for parametrizing the OH rate constants based on the type and position of the methyl and ethyl substituents on the pyridine ring has been constructed, and similar accuracy to that previously obtained for benzene derivative rate data is achieved. Transition state theory calculations have been performed to explore the substituent effect on the observed OH rate constants. The atmospheric implications of the findings are discussed in terms of the role of pyridinated compounds in the ionic composition of the troposphere.

Introduction

The ion content of the troposphere is important because it influences the electrical conductivity of the atmosphere, and it has been proposed that ion recombination processes could be a source of ultrafine aerosol particles.[1] These ultrafine aerosol particles are believed to be important in the regulation of the Earth's climate through their role as cloud condensation nuclei.[2] Some 20 years ago, Eisele reported the first ground level ion composition measurements. These observations revealed the presence of positive ions with masses of 80 and 94 amu.[3] Improved measurement techniques eventually led to the identification of these ionic species as the protonated ions of the aromatic compounds pyridine (C_5H_5N) and picoline (or methylpyridine, $C_5H_4(CH_3)N$), respectively. In addition, a third ion in the series with mass 108 amu was identified as arising from the protonated ions of lutidine (or dimethylpyridine; $C_5H_3(CH_3)_2N$) and/or ethylpyridine ($C_5H_4(C_2H_5)N$).[4] The atmospheric source of the neutral precursors of these tropospheric ions remains somewhat uncertain; however, these compounds have been observed as products of coal combustion[5] and tobacco burning.[6] Although pyridinated ions were found to dominate in many different environments, $NH_4^+(H_2O)_n$ ions have been found to be the predominant positive tropospheric ions in some locations.[7] Several other positive ions (such as protonated di- and trimethylamine, isobutylamine, and quinoline) have now been identified via ground level measurements.[8] In addition, positive ions arising from the protonation of acetone and acetonitrile are believed to dominate in the upper troposphere.[9]

Recently, a chemical model of tropospheric ion composition was proposed, which attempted to provide a mechanistic foundation for the prediction of ionic concentrations in the atmosphere.[10] While the model was successful in some respects, the authors noted that the lack of knowledge concerning the ion−molecule chemistry and the concentrations of the neutral precursors limited the utility of the model results. The atmospheric lifetimes of the neutral precursor compounds play a large role in determining the observed ion composition, as more the persistent neutral compounds are more likely to participate in ion-forming chemical processes. In particular, the pyridinated ions showed a strong spatial variation (concentrations were predicted to be much lower in locations remote from the sources) in the model, due to the presumed short lifetimes of these compounds. This presumption was based on an experimental measurement of the lifetime of pyridine (through measurement of the OH + pyridine reaction rate constant). However, as the lifetimes for the picolines, lutidines, and ethylpyridines had not been experimentally determined, they were estimated by extrapolating the substituent dependence observed for methyl- and ethyl-substituted benzene compounds.

Atkinson and co-workers have developed an empirical structure−reactivity relationship (SRR) model for the prediction of OH rate constants for a number of gas-phase organic compounds.[11] In this model, it is assumed that OH reactions proceed by four possible additive pathways (H-atom abstraction, OH addition to unsaturated C−C bonds, OH addition to aromatic rings, and OH interaction with N-, S-, and P-containing groups). The SRR model successfully reproduces (within a factor of 2) the room-temperature experimental OH rate constants for 90% of the 485 organic compounds used to determine the empirical parameters. However, as there are very little data on the kinetics of OH reactions with heterocyclic compounds, no SRR predictions are available for pyridine and its derivatives.

Recently, Hadad and co-workers used transition state theory (TST) to study the reaction of H, O, and OH with monocyclic aromatic hydrocarbons in an effort to understand the relative importance of the H-atom abstraction and addition pathways, as well as the attack site preferences for these compounds.[12] It was found that the OH-addition to the aromatic ring channel was dominant at room temperature for the reaction of OH with pyridine (with the abstraction channel becoming important at higher temperatures), and that the meta attack site was preferred (the transition state barrier was found to be roughly 2 kcal/mol lower than the nearly exoergic ortho and para barriers to reaction). The reaction of OH at the aromatic nitrogen position was found to highly unfavorable. However, since pyridine was

* E-mail: matthew.elrod@oberlin.edu. Telephone: (440) 775-6583. FAX: (801) 697-4917.

10.1021/jp027389s CCC: $25.00
Published on Web 05/09/2003

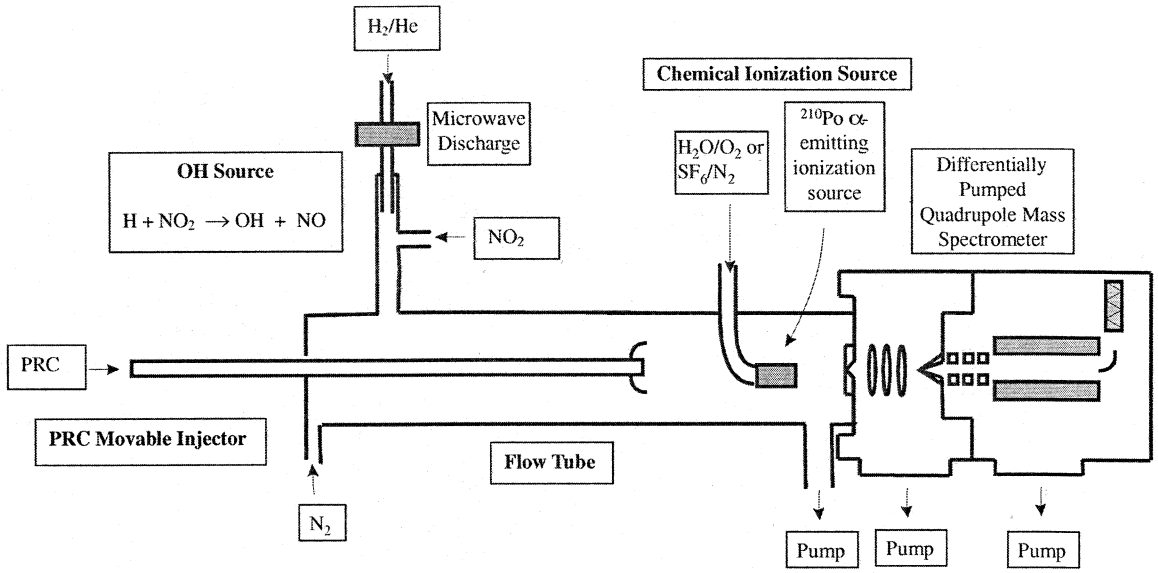

Figure 1. Experimental apparatus.

the only aromatic heterocyclic compound studied in this work, no conclusions concerning substituent effects on the OH rate constants were made.

In this paper, we describe our experimental investigation into the kinetics of the reaction between OH and pyridine, all three picoline isomers, all six lutidine isomers, and all three ethylpyridine isomers. The experiments were conducted at pressures near 100 Torr and at 298 K using a turbulent flow (TF) tube coupled to a high-pressure chemical ionization mass spectrometer (CIMS). We also derive a structure−reactivity relationship model which reproduces the experimental OH rate constants for pyridine and its derivatives as well or better than as the previously determined SRR model for benzene and its derivatives.[11] In addition, we use transition state theory calculations in an effort to better understand the substituent effects on the observed OH rate constants. Finally, the atmospheric implications of the results are discussed.

Experimental Procedures

Turbulent Fast Flow Kinetics. A schematic of the experimental apparatus is presented in Figure 1 and is similar to that used in our previous study of $C_2H_5O_2 + NO_x$.[13] The flow tube was constructed with 2.2 cm i.d. Pyrex tubing and was 100 cm in total length. A large flow of nitrogen carrier gas (approximately 30 STP L min^{-1}) was injected at the rear of the flow tube. The gases necessary to generate OH were introduced though a 10-cm long 12.5-mm diameter sidearm located at the rear of the tube. The pyridine-related compounds (future references to a nonspecific pyridine-related compound reactant will be abbreviated PRC) were added via an encased movable injector. The encasement (made from corrugated Teflon tubing) was used so that the injector could be moved to various injector positions without breaking any vacuum seals.. A fan-shaped Teflon device was placed at the end of the injector to enhance turbulent mixing. The polonium-210 alpha-emitting ionization source was placed between the flow tube and the inlet to the CIMS. Most of the flow tube gases were removed at the CIMS inlet by a 31 L s^{-1} roughing pump. All gas flows were monitored with calibrated mass flow meters. The flow tube pressure was measured upstream of the ionization source using a 0−1000 Torr capacitance manometer. The temperature in the flow tube was determined using Cu-constantan thermocouples.

Overall Rate Constant Determination. OH was generated using the following reaction:

$$H + NO_2 \rightarrow OH + NO \quad (1)$$

($k_1 = 1.28 \times 10^{-10}$ cm^3 $molecule^{-1}$ s^{-1}; all rate constant values quoted are for 298 K values unless otherwise indicated).[14] Hydrogen atoms were produced by passing a dilute H_2/He mixture through a microwave discharge produced by a Beenakker cavity operating at 50 W. The dilute H_2/He mixture was obtained by combining a 4.0 STP L min^{-1} flow of helium (99.999%), which had passed through a silica gel trap immersed in liquid nitrogen, with a 1.0 STP mL min^{-1} flow of a 1% H_2 (99.9%)/He mixture. To generate OH, the hydrogen atoms were then injected into a sidearm and mixed with an excess of NO_2 (CP grade, $\sim 2 \times 10^{12}$ molecule cm^{-3}) to ensure that no hydrogen atoms were introduced into the main flow.

Absolute OH concentrations (needed to ensure pseudo first-order kinetics conditions) were determined by the titration of OH with NO_2

$$OH + NO_2 \rightarrow HNO_3 \quad (2)$$

($k_2 = 3.4 \times 10^{-12}$ cm^3 $molecule^{-1}$ s^{-1} at 100 Torr)[14] and calibration of the HNO_3 mass spectrometer signal using a bubbler containing 60% HNO_3 solution by weight, immersed in an ice−water bath. The vapor pressure of HNO_3 for this solution at 0 °C is 0.20 Torr.[15]

Known amounts of PRC were added via the movable injector either by using glass bulbs containing known mixtures of dilute PRC in N_2 (~1%) as a reservoir for flow metered delivery, or by flowing metered N_2 through a trap containing pure PRC. Because of the difficulty of preparing accurate gas mixtures below concentrations of 0.5%, the trap method was preferred for compounds with low vapor pressures. Experiments involving pyridine and the three picolines were performed using the glass bulb addition method, while the experiments involving the six lutidines and the three ethylpyridines were performed using the trap addition method. Depending on the range of convenient concentrations for the OH + PRC kinetic measurements, the trap was either held near room temperature with a water bath or near 0 °C with an ice water bath. To facilitate the calculation of flow tube PRC concentrations, the vapor pressures of the

PRCs were measured at the appropriate temperature using a 0−10 Torr capacitance manometer. The glass bulb and trap addition methods were found to be consistent with each other through rate constant measurements using both methods for the OH + 2,6-lutidine reaction.

Chemical Ionization Mass Spectrometric Detection. A negative ion chemical ionization scheme (with SF_6^- as the reagent ion) was used to detect OH and HNO_3 with the quadrupole mass spectrometer:

$$SF_6^- + OH \rightarrow OH^- + SF_6 \quad (3)$$

$$SF_6^- + HNO_3 \rightarrow F^-HNO_3 + SF_5 \quad (4)$$

($k_3 = 2 \times 10^{-9}$ cm^3 molecule^{-1} s^{-1}, $k_4 = 2.0 \times 10^9$ cm^3 molecule^{-1} s^{-1}).[16,17] SF_6^- was produced in the ionization source by passing a large N_2 flow (7 STP L min^{-1}) and 1.5 STP mL min^{-1} of 10% SF_6/N_2 through the polonium-210 alpha-emitting ionization source. The commercial ionization source consisted of a hollow, cylindrical (69 × 12.7 mm) aluminum body with 10 mCi (3.7×10^8 disintegrations s^{-1}) of polonium-210 coated on the interior walls.

Ions were detected with a quadrupole mass spectrometer housed in a two-stage, differentially pumped vacuum chamber. Flow tube gases (neutrals and ions) were drawn into the front chamber through a charged 0.1-mm aperture. The ions were focused by three lenses constructed from 3.8 cm i.d., 4.8 cm o.d. aluminum gaskets. The front chamber was pumped by a 6 in. 2400 L s^{-1} diffusion pump. The gases entered the rear chamber through a skimmer cone with a charged 1.0-mm orifice, which was placed approximately 5 cm from the front aperture. The rear chamber was pumped by a 250 L s^{-1} turbomolecular pump. After passing through the skimmer cone, the ions were mass filtered and detected with a quadrupole mass spectrometer.

Computational Methods

Transition State Theory Calculations. The potential energy surfaces for the reaction OH with pyridine and its methyl- and ethyl-substituted derivatives were studied using density functional theory, with the Gaussian 98 package used to perform all geometry optimizations and frequency calculations.[18] The geometry of each structure was fully optimized at the B3LYP/6-31G(d,p) level,[19] with this basis set being the largest with which geometry optimizations could be reasonably carried out using the available computational resources. The PRC−OH transition state structures were treated as doublets and were optimized using the Berny algorithm (opt = calcfc). Harmonic vibrational frequencies were calculated for each stationary point to verify the correct number of real and imaginary frequencies and to provide zero-point vibrational energy (ZPE) corrections.

Truhlar and co-workers recently showed that a hybrid Hartree−Fock-density functional model (MPW1K) was successful in producing more accurate reaction barriers than the B3LYP method, and that the use of diffuse basis sets was also important.[20] Thus, single point energies at the MPW1K/6-31+G(d,p)//B3LYP/6-31G(d,p) level were calculated in an effort to obtain more accurate values for the reaction barrier energies.

Following the recent work of Hadad and co-workers on the reaction of H, O, and OH with monocyclic aromatic hydrocarbons,[12] the B3LYP/6-31G(d,p)//B3LYP/6-31G(d,p) and MPW1K/6-31+G(d,p)//B3LYP/6-31G(d,p) transition state energies were used with nonvariational transition state theory and a Wigner estimate for the tunneling correction, $\Gamma(T)$,[21] to calculate reaction rate constants. The following expressions were used:

$$k(T) = \Gamma(T)\frac{k_B T}{Nh}\frac{Q^{\ddagger}_{TS}(T)}{Q_{PRC}(T)Q_{OH}(T)}e^{-E_0/RT} \quad (5)$$

with

$$\Gamma(T) = 1 + \frac{1}{24}\left(\frac{h\nu_i}{k_B T}\right)^2 \quad (6)$$

where $Q^{\ddagger}_{TS}(T)$, $Q_{PRC}(T)$, and $Q_{OH}(T)$ are the total partition functions for the transition state, the PRC reactant, and OH, respectively, at temperature T, k_B is the Boltzmann constant, h is Planck's constant, N is Avogadro's number, E_0 is the reaction barrier energy, R is the gas constant, and ν_i is the imaginary vibrational frequency of the transition state. For OH, the electronic partition function was calculated using the experimental splittings for the low-lying excited states.[22] Using eq 5, calculated rate constants can be directly compared to experimental rate constants. However, the main goal in this work will be to rationalize the relative experimental rate constants (compared to pyridine) for the reaction of OH with the PRCs. This focus on relative rate constants will minimize any effect of systematic error in the calculation of transition state barrier energies.

Results and Discussion

Overall Rate Constant Determination. Bimolecular rate constants were obtained via the usual pseudo first-order approximation method, using the PRC as the excess reagent. In all experiments, the bulk flow velocity was about 1150 cm s^{-1} and the Reynolds number was about 2300. Typical OH concentrations were determined to be $\sim 1.0 \times 10^{11}$ molecule cm^{-3}, which was always more than a factor of 10 less than the PRC concentrations used. In each case, the PRC concentrations were adjusted to achieve first-order rate constants between 10 and 60 s^{-1}. For pyridine, the concentrations ranged from 3×10^{12} to 2×10^{13} molecule cm^{-3}. The OH decay curves were corrected for OH loss on the moveable injector and reaction with NO_2 (reaction 2). Because OH radical loss on the injector decreases at increased injector distances (because less injector surface area is exposed as the injector is pulled back), the background OH "decay" due to this phenomenon will lead to a negative first-order rate constant. Given the 100 Torr, 298 K OH + NO_2 rate constant of 3.4×10^{-12} cm^3 molecule^{-1} s^{-1} and a typical NO_2 concentration of 2.0×10^{12} molecule cm^{-3}, the background OH decay rate due to reaction with NO_2 is estimated to be about 7 s^{-1}. In our experiments, the actual total background OH "decay" was very reproducibly determined to be about −20 s^{-1}. Since this figure represents the sum of OH radical loss on the injector surface as well as reaction with NO_2, we can estimate that the OH "decay" due to radical loss on the injector alone is about −27 s^{-1}. Typical background-corrected OH decay curves as a function of injector distance are shown in Figure 2 for the specific case of the OH + 2,5-lutidine kinetics measurements. The first-order rate constants obtained from fitting the OH decay curves were plotted against [PRC] to determine the bimolecular rate constant, as shown in Figure 3 for the specific case of the OH + 2,5-lutidine. This approach for determining bimolecular rate constants assumes that deviations from the plug flow approximation (molecular velocities are equal to the bulk flow velocity) are negligible. Under the conditions present in our turbulent flow tube (Reynold's Number > 2000), Seeley et al. estimated that these deviations result in apparent rate constants which are at most 8% below the actual

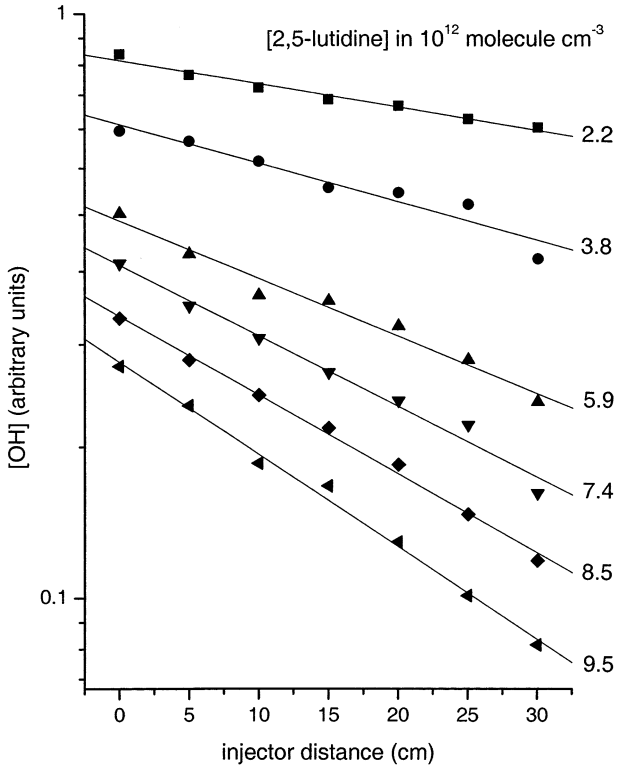

Figure 2. Pseudo first-order OH decay curves for the OH + 2,5-lutidine reaction at 100 Torr, 298 K, 1150 cm s^{-1} velocity, 2300 Reynolds number.

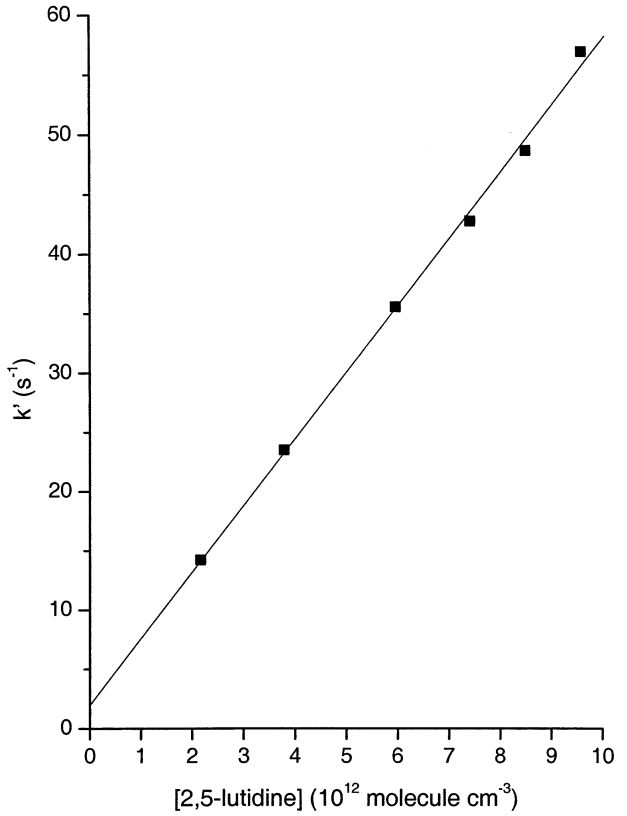

Figure 3. Determination of overall bimolecular rate constant for the OH + 2,5-lutidine reaction from data in Figure 2 ($k = 5.61 \pm 0.28 \times 10^{-12}$ cm^3 $molecule^{-1}$ s^{-1}).

values.[23] The other likely systematic errors in the determination of rate constants are likely to occur in the measurements of gas flows, temperature, detector signal, and pressure. Considering such sources of error, we estimate that rate constants can be determined with an accuracy of ± 30% (2σ).

TABLE 1: Experimental Rate Constants and Calculated Atmospheric Lifetimes

compound	no. of trials	PRC method	k (10^{-12} cm^3 $molecule^{-1}$ s^{-1})[a]	lifetime (days)[b]
pyridine	4	bulb	0.531 ± 0.060	43.6
2-picoline	3	bulb	2.79 ± 0.26	8.30
3-picoline	3	bulb	2.30 ± 0.24	10.1
4-picoline	4	bulb	2.69 ± 0.46	8.60
2,3-lutidine	3	trap	4.9 ± 1.1	4.74
2,4-lutidine	2	trap	19.0 ± 3.4	1.22
2,5-lutidine	5	trap	5.61 ± 0.28	4.12
2,6-lutidine	4	bulb/trap	8.88 ± 0.56	2.60
3,4-lutidine	3	trap	3.05 ± 0.42	7.58
3,5-lutidine	2	trap	4.41 ± 0.48	5.24
2-ethylpyridine	2	trap	7.10 ± 0.82	3.26
3-ethylpyridine	2	trap	3.59 ± 0.62	6.44
4-ethylpyridine	3	trap	3.89 ± 0.40	5.96

[a] 2σ error limits indicated. [b] Atmospheric lifetimes calculated assuming [OH] = 1.0×10^6 molecule cm^3 and 12 h diurnal cycle.

At least two separate determinations of the rate constant at 100 Torr and 298 K for the reaction of OH with each PRC were carried out. Table 1 contains the experimentally measured rate constant for each PRC species; the stated uncertainty represents the two standard deviation statistical error in the data and is not an estimate of systematic errors. Our OH + pyridine rate constant is in excellent agreement with the previously determined value of 4.9×10^{-13} cm^3 $molecule^{-1}$ s^{-1} measured at 735 Torr and 296 K.[24] To the best of our knowledge, there exist no other literature data for the kinetics for the reaction of OH with the other PRCs examined in this work.

Structure−Activity Relationship Model. A structure reactivity relationship (SRR) model for the PRCs studied in this work was constructed by modifying the prescription of Kwok and Atkinson.[11] In this model, it is assumed that the total rate constant is the sum of the OH addition to the aromatic ring rate constant and the H-atom abstraction by OH from alkyl groups rate constant

$$k_{tot} = k_{add} + k_{abs} \quad (7)$$

where k_{abs} is equal to 1.36×10^{-13} cm^3 $molecule^{-1}$ s^{-1} for H-atom abstraction by OH for each methyl group bonded to the aromatic ring and k_{abs} is equal to 1.10×10^{-12} cm^3 $molecule^{-1}$ s^{-1} for H-atom abstraction by OH for each ethyl group bonded to the aromatic ring. The abstraction of aromatic hydrogens by OH is considered to be of minor importance and is negelected in the model.[11] The rate constant for OH addition to the aromatic ring is calculated from a Hammett equation-based approach:

$$\log k_{add} = \log k_0 + \sigma\rho \quad (8)$$

where k_0 is the rate constant for OH addition to the aromatic ring for the unsubstituted aromatic compounds, σ is a constant characteristic of the substituent, and ρ is a constant for the particular reaction that is a measure of the sensitivity of the reaction to substituent changes. In the case of electrophilic aromatic substitution reactions (such as the OH addition reactions under study here), σ in eq 8 is actually the sum of the experimentally determined electrophilic substituent constants ($\Sigma\sigma^+$) as compiled by Brown and Okamoto.[25] Each substituent has a corresponding constant for either addition at the ortho or para position (these positions are constrained to be equivalent and are assigned a single value, σ^+_{o-p}) or for addition at the

TABLE 2: Calculated Structure−Reactivity Relationship (SRR) Rate Constants Using Nitrobenzene SRR Parameters and Modified SRR Parameters Fitted to Experimental Data

compound	nitrobenzene SRR k (10^{-12} cm^3 molecule^{-1} s^{-1})	modified SRR k (10^{-12} cm^3 molecule^{-1} s^{-1})
pyridine	0.24	0.80
2-picoline	0.77	3.24
3-picoline	0.58	2.01
4-picoline	0.77	3.24
2,3-lutidine	1.05	4.41
2,4-lutidine	1.93	12.27
2,5-lutidine	1.05	4.41
2,6-lutidine	1.93	12.27
3,4-lutidine	1.05	4.41
3,5-lutidine	1.43	7.52
2-ethylpyridine	1.71	4.00
3-ethylpyridine	1.52	2.85
4-ethylpyridine	1.71	4.00

meta position (σ_m^+). As discussed by Zetzsch,[26] $\Sigma\sigma^+$ is calculated by assuming that (a) steric hindrance can be neglected, (b) $\Sigma\sigma^+$ is the sum of all of the substituent constants of the substituent groups attached to the aromatic ring, (c) the OH radical adds to the position yielding the most negative value of $\Sigma\sigma^+$, and (d) if all positions on the ring are occupied, the ipso position is treated as the meta position. For example, for the case of OH addition to 4-methyl nitrobenzene, the relevant electrophilic aromatic substituent constants are σ_{o-p}^+ (methyl) $= -0.311$, σ_m^+ (methyl) $= -0.066$, σ_{o-p}^+ (nitro) $= 0.790$, and σ_m^+ (nitro) $= 0.674$.[25] Therefore, the OH addition would occur at the 3-position, since this would minimize the value of $\Sigma\sigma^+$ ($\Sigma\sigma^+ = \sigma_{o-p}^+$ (methyl) + σ_m^+ (nitro) for this case). For the case of OH reaction with benzene and biphenyl, Atkinson and Kwok have fitted experimental data (usually to within a factor of 2) to values of log k_0 of -11.71 and ρ of -1.34. For the case of heterocyclic aromatic compounds such as those under study, there does not exist a similar set of electrophilic aromatic substituent constants, although there have been previous, largely unsuccessful, efforts to determine these constants for some pyridine derivatives.[27]

To implement a SRR model for the OH + PRC reactions under study here, we have instead chosen to represent the aromatic nitrogen atom as a substituent itself to allow use of existing electrophilic aromatic substituent constants for benzene. Our initial attempts involved trying to determine, via least-squares fitting to our data for pyridine and the twelve other PRCs, values for all unknown constants necessary to calculate the rate constant from eq 7: σ_{o-p}^+ (N, aromatic) and σ_m^+ (N, aromatic), log k_0, and ρ. However, we found that our data set was not sufficient to simultaneously determine all four parameters. By a trial-and-error approach, we found that using the electrophilic aromatic substituent constants for nitrobenzene (i.e., treating the aromatic nitrogen atom in the PRCs as a nitro substituent) as surrogates for σ_{o-p}^+ (N, aromatic) and σ_m^+ (N, aromatic), we were able to fit log k_0 and ρ satisfactorily to our 13 experimental OH rate constants with values of -10.82 and -1.89, respectively. Table 2 lists the calculated SRR OH + PRC rate constants using the Kwok and Atkinson values for log k_0 and ρ, and our fitted values for log k_0 and ρ and the electrophilic aromatic substituent constants for nitrobenzene. Comparison of these calculated rate constants to the experimental values in Table 1 shows that the modified SRR model performs much better, and that all rate constants are within a factor of 1.6 (most are in much better agreement) of the experimental values. This accuracy is similar or better to that achieved by Atkinson and Kwok for the reaction of OH with substituted benzene compounds.[11] However, the SRR model treats the ortho and para positions as equivalent, and it is clear from the experimental data given in Table 1 (particularly for the lutidines and ethylpyridines) that this is clearly not actually the case. Therefore, we undertook transition state theory calculations to explore the full complexity of the substituent effects.

Transition State Theory Calculations. The 13 PRC compounds, OH, and 40 unique OH−PRC transition state structures resulting from OH addition to the aromatic ring for the PRC compounds were determined via optimization at the B3LYP/6-31G(d,p) level and are available as Supporting Information. In every case, the OH molecule adds to the aromatic ring such that the O atom is located almost directly above the carbon atom on the aromatic ring and the H atom points toward the center of the aromatic ring at a distance slightly further above the ring than the O atom. This is the same transition state structure found by Hadad and co-workers for OH + pyridine.[12] All aromatic ring addition positions were studied, except for OH attack at the aromatic nitrogen position and at the ipso position. Hadad and co-workers had previously found that the OH addition at the aromatic nitrogen in pyridine was highly unfavorable. To confirm this result, we calculated the TST reaction barrier for OH addition to the aromatic nitrogen atom in pyridine and found that barrier is more than 15 kcal mol^{-1} higher than the barrier for the most favorable OH addition site (the 3-position). Therefore, OH addition at the aromatic nitrogen atom was neglected in the calculation of the TST rate constants. We calculated the TST rate constant for ipso attack on 4-picoline, and found it was about 0.5% of the sum of the rate constants for the open ring addition positions. It is clear from the difficulty encountered in finding the transition state for this species, as well as from the difference in the OH orientation in the final optimized structure as compared to attack at the open ring sites, that steric effects play a role in reducing the attractiveness of the ipso site for OH addition. Therefore, due to the very minimal calculated contribution of reaction at the ipso position to the overall rate constant for the case of 4-picoline, addition at the ipso was neglected in the other TST calculations. The rotational constants, vibrational frequencies, zero point energies, B3YLP/6-31G(d,p) and MPW1K/6-31+G(d,p) energies are also available as Supporting Information. Table 3 contains the calculated TST rate constants for calculations using either the B3YLP/6-31G(d,p) or MPW1K/6-31+G(d,p) barrier heights.

The TST rate constants may be compared to experimental values by summing the rate constants calculated at each possible OH addition position. Note that the TST rate constants are for the addition mechanism only; however, the experimental data used to derive the benzene SRR model predicts that the abstraction mechanism should be significant only for the reaction of OH with the ethylpyridines (only about 20% of the total rate constant). Therefore, we expect that the substituent effects observed in the experimental data should be largely captured by a TST treatment of the addition mechanism only. The absolute B3LYP/6-31G(d,p) TST rate constant values are in remarkable, and probably coincidental, agreement with the experimental rate constants. On the other hand, the MPW1K/6-31+G(d,p) TST rate constant values are much lower than experimental values, which is largely due to the fact that this method systematically results in barrier heights about 5 kcal mol^{-1} higher than the B3LYP/6-31G(d,p) method. Hadad and co-workers also reported about a 5 kcal mol^{-1} higher barrier height for MPW1K as compared to B3LYP calculations for the reaction of OH with series of heterocyclic compounds.[12]

TABLE 3: Calculated Barrier Heights (kcal mol^{-1}) and Transition State Theory Rate Constants (cm^3 molecule^{-1} s^{-1})[a]

		B3LYP/6-31G(d,p)		MPW1K/6-31+G(d,p)	
compound	site	E_0	10^{-13} k	E_0	10^{-17} k
pyridine	2	0.39	0.39	5.53	0.67
	3	−1.11	5.17	3.32	28.71
	4	0.40	0.42	4.99	1.78
2-picoline	3	−2.68	27.18	2.03	94.01
	4	0.41	0.32	5.04	1.25
	5	−1.73	12.20	2.79	58.20
	6	0.04	0.59	5.29	0.82
3-picoline	2	−1.71	5.86	2.39	56.94
	4	−1.33	2.29	3.31	8.91
	5	−1.11	4.11	3.26	25.27
	6	−0.30	2.21	4.66	5.01
4-picoline	2	0.39	0.22	5.44	0.42
	3	−2.63	16.73	1.96	70.91
2,3-lutidine	4	−0.70	3.83	3.78	19.45
	5	−1.80	17.35	2.62	98.73
	6	−0.59	2.06	4.43	4.24
2,4-lutidine	3	−4.10	94.05	0.78	245.61
	5	−3.10	33.81	1.74	94.46
	6	−0.01	0.52	5.15	0.84
2,5-lutidine	3	−2.75	24.87	1.91	95.87
	4	−1.37	1.36	3.29	5.14
	6	−2.02	10.45	2.10	97.88
2,6-lutidine	3	−3.26	34.96	1.52	106.62
	4	0.42	0.14	5.02	0.58
3,4-lutidine	2	−1.27	9.66	2.78	101.97
	5	−1.99	38.01	2.37	235.90
	6	−0.19	1.23	4.79	2.67
3,5-lutidine	2	−2.41	18.66	1.64	196.89
	4	−2.97	46.29	1.76	154.98
2-ethylpyridine	3	−2.64	25.00	2.66	31.93
	4	0.35	0.38	4.92	1.66
	5	−1.72	13.77	2.76	71.14
	6	0.13	0.58	5.28	0.97
3-ethylpyridine	2	−1.40	3.11	4.07	2.95
	4	−1.18	2.51	4.29	2.38
	5	−1.24	5.27	3.18	29.87
	6	−0.24	1.18	4.81	2.31
4-ethylpyridine	2	0.19	0.64	5.24	1.25
	3	−2.78	37.68	2.77	31.68

[a] Reactant and transition state structures were determined via B3LYP/6-31G(d,p) optimization.

Although they found that their MPW1K barriers also lead to underestimates of the rate constants, their MPW1K results were in better agreement with experimental values than their B3LYP results.

On a fundamental level, the TST results support the SRR picture for the determination of the preferred site for OH addition. For example, the 3-position is very much more favorable than other positions for OH addition to pyridine because of the meta-directing nature of the relatively electronegative substituent. For 2-picoline, the 3-position is also easily the most favorable for OH addition because the methyl substituent reinforces the preference for the 3-position. Note also that the 5-position is equivalent to the 3-position in the SRR model, but is slightly less favorable in the TST calculation. However for 3-picoline, the methyl substituent destabilizes the preference for the 3-position (this also shows up in the total OH addition rate constant for 3-picoline, which is lower than either 2- or 4-picoline), and all four possible positions have very similar calculated TST rate constants. In cases where the substituent effects reinforce the attack site preference, the TST results indicate that the simple SRR picture is largely valid. However, in cases where the substituent effects are at odds, the TST results indicate that several OH addition positions can be competitive, as opposed to the SRR requirement of one largely favored addition position.

TABLE 4: Comparison of Experimental and Calculated Relative Rate Constants[a]

compound	exp	modified SRR	TST B3LYP/6-31G(d,p)	TST MPW1K/6-31+G(d,p)
pyridine	1	1	1	1
2-picoline	5.25	4.04	6.72	4.98
3-picoline	4.33	2.50	2.41	3.10
4-picoline	5.07	4.04	5.66	4.60
2,3-lutidine	9.19	5.49	3.88	3.95
2,4-lutidine	35.78	15.30	21.42	10.99
2,5-lutidine	10.56	5.49	6.12	6.41
2,6-lutidine	16.72	15.3	11.69	6.89
3,4-lutidine	5.74	5.49	8.16	10.98
3,5-lutidine	8.31	9.37	13.95	17.70
2-ethylpyridine	13.37	4.98	6.63	3.41
3-ethylpyridine	6.76	3.55	2.01	1.21
4-ethylpyridine	7.33	4.98	12.78	2.12

[a] Relative to pyridine.

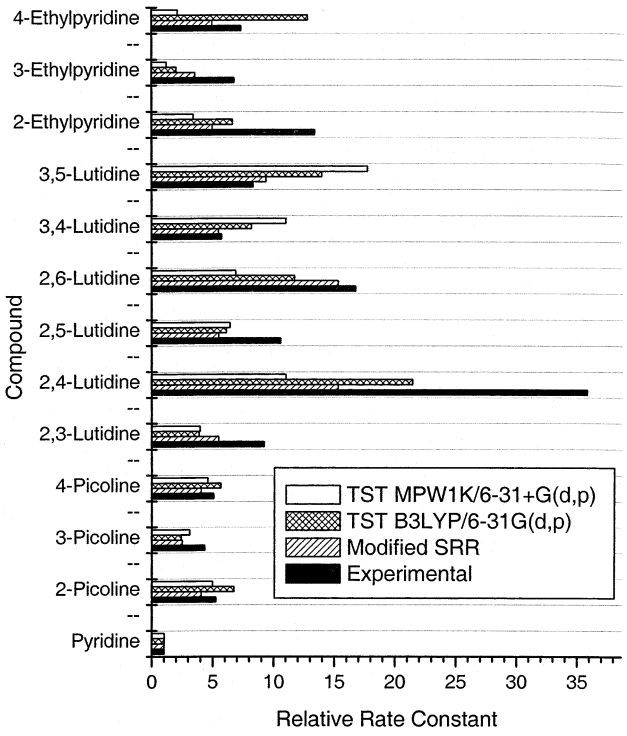

Figure 4. Comparison of experimental and calculated relative rate constants (relative to pyridine).

To more easily explore the substituent effects observed in the rate constants, it is convenient to compare experimental, SRR and TST rate constants values relative to their respective values for pyridine, the base compound of the species under study. Table 4 and Figure 4 contain such a comparison for relative experimental, modified SRR, B3LYP/6-31G(d,p) TST, and MPW1K/6-31+G(d,p) TST rate constants. As a group, the SRR results successfully reproduce the experimental observation of increasing OH reaction rate constants: $k_{\text{pyridine}} < k_{\text{picolines}} < k_{\text{ethylpyridines}} < k_{\text{lutidines}}$. Also, within the SRR limitation of ortho and para positions being equivalent, the SRR results are reasonably accurate for the trends observed within the picoline, lutidine, and ethylpyridine families. However, the ortho-para equivalence assumption in the SRR model is proven inadequate for the SRR-equivalent sets of (i) 2,3-lutidine, 2,5-lutidine, and 3,4-lutidine, (ii) 2,4-lutidine and 2,6-lutidine, and (iii) 2-ethylpyridine and 4-ethylpyridine. All three sets show variations

of up to a factor of 2 in the experimental rate constant, depending on the specific PRC.

The B3LYP/6-31G(d,p) TST results are also generally successful in reproducing the experimentally observed increase in OH rate constants: $k_{\text{pyridine}} < k_{\text{picolines}} < k_{\text{ethylpyridines}} < k_{\text{lutidines}}$. The B3LYP/6-31G(d,p) TST results also reproduce the experimental trend observed within the picolines: a markedly smaller rate constant for 3-picoline and a slightly larger rate constant for 2-picoline relative to 4-picoline. However, the results are more mixed for the lutidines and ethylpyridines. The SRR-equivalent compounds (sets 1 and 3 from above) are predicted to have different rate constants, but the experimental patterns are not reproduced by the TST calculations. The B3LYP/6-31G(d,p) TST method does successfully predict the experimental pattern observed for set 2, however, as 2,4-lutidine is predicted to have the largest OH rate constant of any of the PRCs studied (as is experimentally observed). The relative rate constants predicted from the MPW1K/6-31+G(d,p) method are fairly similar to the B3LYP/6-31G(d,p) results, but are even less successful in predicting the substituent trends observed within the lutidines. It is unclear why the MPW1K method performs more poorly than the B3LYP method for these systems.

Atmospheric Implications. In Table 1, the atmospheric lifetimes of the 13 PRC compounds studied are reported, assuming removal by gas-phase OH reaction only, an average OH concentration of 1.0×10^6 molecule cm^{-3}, and a 12 h diurnal cycle. The calculated lifetimes range from almost 44 days for pyridine to a little more than 1 day for 2,4-lutidine. As noted in the introduction, it is expected that the longer the lifetime of neutral precursor compounds, the more likely they will persist long enough to be involved in ion-forming processes. It is therefore useful to compare the lifetimes of the PRC compounds with the lifetimes of neutral precursors also known to participate in ion-formation chemistry. Of the observed tropospheric ions discussed in the introduction, the OH rate constants have been measured for the precursor compounds ammonia, acetone, and acetonitrile,[14] and the corresponding lifetimes are 145, 105, and 1010 days. These lifetimes are probably conservative as they are based on gas phase removal by OH only. This is particularly true for NH_3, where dry deposition is known to be important. Nonetheless, the PRC compounds show strikingly shorter atmospheric lifetimes, with pyridine being the only compound with a lifetime in excess of 10 days. As discussed by Beig and Brasseur, short neutral precursor lifetimes such as those determined for the PRCs studied here should be manifested in observations of local variation in pyridinated ion concentration.[10] These results also suggest that the ion formation processes for the PRCs must also be very kinetically efficient, since the neutral precursors are relatively transient compared to ammonia, acetone, and acetonitrile. Viggiano and co-workers have investigated some of the possible ion forming pathways for pyridine and the picolines and have found that these reactions do indeed occur near the collision-limited rate.[28,29] However, the similar ion forming reactions for ammonia, acetone, and acetonitrile were also found to be very fast.[28,29] Since these results show that the kinetics of removal of the neutral precursor compounds are faster for the PRCs than for ammonia, acetone, or acetonitrile and it has been previously shown that the ion formation rates are similar for all species,[8] it seems unlikely that kinetic effects are responsible for the observation of significant concentrations of pyridinated ions. However, because the PRCs have significantly larger proton affinities than ammonia, acetone, or acetonitrile, the contention that the ubiquitous presence of pyridinated ions is strongly controlled by thermodynamic driving forces remains as the most reasonable explanation for the observed phenomenon.

Conclusions

The results of the experimental investigation of the kinetics of the reaction of OH withpyridine, all three picoline isomers, all six lutidine isomers, and all three ethylpyridine isomers at 100 Torr pressure and 298 K were interpreted in terms of an empirical structure−reactivity relationship (SRR) model and transition state theory (TST). The general substitution trend in the experimental rate constants (in increasing rate constant order: $k_{\text{pyridine}} < k_{\text{picolines}} < k_{\text{ethylpyridines}} < k_{\text{lutidines}}$) are well reproduced by both the SRR model (using nitrobenzene as a surrogate for pyridine in the model derived by Kwok and Atkinson[11]) and the TST results. The trends in the experimental rate constants for specific isomers within a particular substituent family are not well captured by the SRR model (which is inherently approximate with respect to this property). The TST results are somewhat better in this respect, but the TST results for the lutidine isomer dependence were generally not in agreement with experimental results. Using the OH reaction rate constants, the atmospheric lifetimes of these compounds were found to be short relative to the neutral precursors of other abundant tropospheric ions (such as ammonia, acetone, acetonitrile). These results suggest that the kinetics of the ion formation processes might be so facile that thermodynamic driving forces play a more significant role in determining the observed tropospheric ionic composition.

Acknowledgment. This material is based upon work supported by the National Science Foundation under Grant No. 0196205.

Supporting Information Available: Optimized geometries, energies, rotational constants, and vibrational frequencies. This material is available free of charge via the Internet at http://pubs.acs.org.

References and Notes

(1) Yu, F.; Turco, R. P. *Geophys. Res. Lett.* **2000**, *27*, 883.
(2) Charlson, R. J.; Lovelock, J. E.; Andreae, M. O.; Warren, S. G. *Nature* **1987**, *326*, 655.
(3) Eisele, F. L. *Int. J. Mass Spectrom. Ion Phys.* **1983**, *54*, 119.
(4) Eisele, F. L. *J. Geophys. Res.* **1988**, *93*, 716.
(5) Clemo, G. R. *Tetrahedron* **1973**, *29*, 3987.
(6) Saint-Jalm, Y. *J. Chromatgr.* **1980**, *198*, 188.
(7) Tanner, D. J.; Eisele, F. L. *J. Geophys. Res.* **1991**, *96*, 1023.
(8) Eisele, F. L.; Tanner, D. J. *J. Geophys. Res.* **1990**, *95*, 20539.
(9) Knop, G.; Arnold, F. *Geophys. Res. Lett.* **1987**, *14*, 1262.
(10) Beig, G.; Brasseur, G. P. *J. Geophys. Res.* **2000**, *105*, 22671.
(11) Kwok, E. S. C.; Atkinson, R. *Atmos. Environ.* **1995**, *29*, 1685.
(12) Barckholtz, C.; Barckholtz, T. A.; Hadad, C. M. *J. Phys. Chem. A* **2001**, *105*, 140.
(13) Ranschaert, D. L.; Schneider, N. J.; Elrod, M. J. *J. Phys. Chem. A* **2000**, *104*, 5758.
(14) DeMore, W. B.; Sander, S. P.; Howard, C. J.; Ravishankara, A. R.; Golden, D. M.; Kolb, C. E.; Hampson, R. F.; Kurylo, M. J.; Molina, M. J. *Chemical Kinetics and Photochemical Data for Use in Stratospheric Modeling, JPL Publication 97−4*, Jet Propulsion Laboratory: Pasadena, California, 1997.
(15) Fritz, J. J.; Fuget, C. R. *Chem. Eng. Data Ser.* **1956**, *1*, 10.
(16) Lovejoy, E. R.; Murrells, T. P.; Ravishankara, A. R.; Howard, C. J. *J. Phys. Chem.* **1990**, *94*, 2386.
(17) Huey, L. G.; Hanson, D. R.; Howard, C. J. *J. Phys. Chem.* **1995**, *99*, 5001.
(18) Frisch, M. J.; Trucks, G. W.; Schlegel, H. B.; Scuseria, G. E.; Robb, M. A.; Cheeseman, J. R.; Zakrzewski, V. G.; Montgomery, J. A., Jr.; Stratmann, R. E.; Burant, J. C.; Dapprich, S.; Millam, J. M.; Daniels, A. D.; Kudin, K. N.; Strain, M. C.; Farkas, O.; Tomasi, J.; Barone, V.; Cossi, M.; Cammi, R.; Mennucci, B.; Pomelli, C.; Adamo, C.; Clifford, S.;

Ochterski, J.; Petersson, G. A.; Ayala, P. Y.; Cui, Q.; Morokuma, K.; Malick, D. K.; Rabuck, A. D.; Raghavachari, K.; Foresman, J. B.; Cioslowski, J.; Ortiz, J. V.; Stefanov, B. B.; Liu, G.; Liashenko, A.; Piskorz, P.; Komaromi, I.; Gomperts, R.; Martin, R. L.; Fox, D. J.; Keith, T.; Al-Laham, M. A.; Peng, C. Y.; Nanayakkara, A.; Gonzalez, C.; Challacombe, M.; Gill, P. M. W.; Johnson, B. G.; Chen, W.; Wong, M. W.; Andres, J. L.; Head-Gordon, M.; Replogle, E. S.; Pople, J. A. *Gaussian 98*, revision A.7; Gaussian, Inc.: Pittsburgh, PA, 1998.

(19) Becke, A. D. *J. Chem. Phys.* **1993**, *98*, 5648.

(20) Lynch, B. J.; Fast, P. L.; Harris, M.; Truhlar, D. G. *J. Phys. Chem. A* **2000**, *104*, 4811.

(21) Wigner, E. P. *Z. Phys. Chem.* **1932**, *B19*, 203.

(22) Noggle, J. H. *Physical Chemistry*, 4th ed.; Little, Brown and Company: Boston, 1985.

(23) Seeley, J. V.; Jayne, J. T.; Molina, M. J. *Int. J. Chem. Kinet.* **1993**, *25*, 571.

(24) Atkinson, R.; Tuazon, E. C.; Wallington, T. J.; Aschmann, S. M.; Arey, J.; Winer, A. M.; Pitts, J. N. *Environ. Sci. Technol.* **1987**, *21*, 64.

(25) Brown, H. C.; Okamoto, Y. *J. Am. Chem. Soc.* **1958**, *80*, 4979.

(26) Zetsch, C. 14th Informal Conference on Photochemistry, Newport Beach, CA, March 30−April 3, 1980.

(27) Noyce, D. S.; Virgilio, J. A.; Bartman, B. *J. Org. Chem.* **1973**, *38*, 2657.

(28) Viggiano, A. A.; Morris, R. A.; Dale, F.; Paulson, J. F. *J. Geophys. Res.* **1988**, *93*, 9534.

(29) Viggiano, A. A.; Dale, F.; Paulson, J. F. *J. Chem. Phys.* **1988**, *88*, 2469.